Exponential Temperature Effects on Skyrmion-Skyrmion Interaction

Yu Wang,[1,*] Jie Wang,[2,3] Takayuki Kitamura,[1] Hiroyuki Hirakata,[1] and Takahiro Shimada[1]

[1] *Department of Mechanical Engineering and Science, Kyoto University, Nishikyo-ku, Kyoto 615-8540, Japan*

[2] *Department of Engineering Mechanics, Zhejiang University, Hangzhou 310027, China*

[3] *Zhejiang Laboratory, Hangzhou 311100, China*

(Received 18 May 2022; revised 30 July 2022; accepted 15 September 2022; published 11 October 2022)

Understanding the dynamic behaviors of magnetic skyrmions has great potential in the application of spintronics. This is especially the case for the interaction between two skyrmions. In the literature, the attractive and repulsive skyrmion-skyrmion interactions are demonstrated as strongly related to the distance of two skyrmions and external magnetic fields. However, as a natural property, the temperature effect on skyrmion-skyrmion interactions is unclear, which lacks understanding from thermodynamics, and accordingly its driving force equation is absent. Here, we employ a temperature-related phase-field simulation and demonstrate that the skyrmion-skyrmion interaction is dramatically changed by temperature (e.g., a temperature change of only a few kelvins results in an eightfold higher interaction), which can lead to critical temperature behavior of skyrmion phase. Detailed analysis shows the interaction potential decreases exponentially with an increase of temperature, and this pronounced temperature dependence originates from the temperature-related skyrmion structure. Then, an equation is proposed to describe the skyrmion interaction at finite temperatures. Therefore, this study provides a deeper understanding of the skyrmion kinetic behavior and explores the temperature control of skyrmion interactions coupled with other sources of interaction, which is a guidance for future study of skyrmions and their applications.

DOI: 10.1103/PhysRevApplied.18.044024

I. INTRODUCTION

A magnetic skyrmion, a local swirl configuration of magnetizations [1,2], is mainly stabilized by the Dzyaloshinskii-Moriya interaction (DMI) [3,4] that comes from a lack of inversion symmetry of magnetic systems and contributes chiral domain walls. Due to its topologically stable structure [5], a skyrmion is regarded as a quasiparticle with topological charge [6,7] $Q = \pm 1$ that is defined as $Q = (1/4\pi) \int \mathbf{M} \cdot (\partial \mathbf{M}/\partial x \times \partial \mathbf{M}/\partial y) dxdy$, where $\mathbf{M}$ is magnetization. Therefore, skyrmions become promising data carriers in future memory devices [8,9] due to their unique particle characters. Examples of such characters are skyrmion-skyrmion interactions [10–17], dynamic motions driven by spin currents [18–21] or gradient fields (such as temperature [22–24], magnetic [25], and strain fields [26–28]), and the skyrmion Hall effect [29] during motions. Especially, the skyrmion-skyrmion interaction is a fundamental behavior between isolated skyrmions and essential for the understanding of related applications. The skyrmion interaction is demonstrated as strongly related to the distance d between two isolated skyrmions. When d is pushed under a critical value, skyrmions show an attractive interaction, in which two skyrmions merge to one skyrmion [14,16]. When d is larger than the critical value, the repulsive interaction is dominant [10,11], in which two skyrmions repel each other to further increase d until stable. In fact, the attractive interaction is weak in thin films [13], and usually suppressed by the repulsive interaction [17]. Therefore, the repulsive skyrmion-skyrmion interaction becomes the main interest. In experiments, magnetic-field-dependent skyrmion interaction is observed in FeGe nanostripes [15]. In theory, the interaction potential U is proposed to quantificationally evaluate the repulsive force of isolated skyrmions [30,31], and the interaction potential U is demonstrated to decrease exponentially with the distance of skyrmions d [13,14]. Accordingly, the equation of the particle model is proposed in exponential form as $U(d) \propto \exp(-d/\lambda)$, where $\lambda \propto 1/\sqrt{|H|}$ is a parameter related to the external magnetic field [14].

Nevertheless, as a natural property, the temperature effect on skyrmion-skyrmion interaction is still unclear. However, temperature is demonstrated to play an important role in skyrmion behaviors. For example, the stability of skyrmions is temperature dependent [32,33], and the inner structures of skyrmions are different at different temperatures (especially near the Curie temperature, at which there is the precursor effect [1,34–37] that makes magnetizations become "soft" then easy to change), and

*wang.yu.51p@st.kyoto-u.ac.jp

temperature even provides a driving force to skyrmion dynamic motions [22–24]. Therefore, the temperature effect is non-negligible on skyrmion interaction and is the motivation of this work.

By following previous theoretical works, we use interaction potential U as an index to show the intensity of skyrmion-skyrmion interaction. Therefore, the unified Landau theory that explicitly includes the temperature effect inside the free-energy functional is suitable for the scenario. Here, we study the skyrmion-skyrmion interaction at finite temperatures by a temperature-related phase-field simulation based on Ginzburg-Landau theory [38]. Our simulation shows that the temperature can affect the magnetization magnitude and inner structure of skyrmions, and then influence the skyrmion-skyrmion interaction potential U. The energy analysis shows that the interaction potential U decreases exponentially with an increase of temperature. Based on that, we propose an equation to describe the temperature-related skyrmion-skyrmion interaction. Therefore, our study provides the thermodynamic mechanism and a particle model equation for skyrmion interaction at finite temperatures.

II. PHASE-FIELD MODELING

A temperature-included phase-field simulation [22,39,40] is employed here to study the magnetic system. The temporal evolution of magnetization $\mathbf{M}$ is generally described by the Landau-Lifshitz-Gilbert (LLG) equation as [41–43]

$$\frac{\partial \mathbf{M}}{\partial t} = -\gamma \mathbf{M} \times \mathbf{H}_{\text{eff}} + \frac{\alpha}{M_s}\mathbf{M} \times \frac{\partial \mathbf{M}}{\partial t}, \tag{1}$$

where $\mathbf{H}_{\text{eff}} = (-1/\mu_0)(\delta F/\delta \mathbf{M})$ is the effective magnetic field, γ is the gyromagnetic ratio, and α is the Gilbert damping. Based on the Ginzburg-Landau theory, the driving force of the magnetization behaviors is described by the thermodynamic total free energy $F = \int f dv$, in which f is the total free-energy density.

The specific free-energy density in a ferromagnetic (FM) system can be written as

$$f = f_{\text{Landau}} + f_{\text{exch}} + f_{\text{DM}} + f_{\text{mag}} + f_{\text{elas}}, \tag{2}$$

where f_{Landau}, f_{exch}, f_{DM}, f_{mag}, and f_{elas} are the Landau, exchange, DMI, magnetostatic, and elastic energy densities, respectively. Especially, the temperature effect on magnetization is introduced by the Landau energy density [1,38], which can be expressed as

$$f_{\text{Landau}} = a(T - T_c)\mathbf{M}^2 + b\mathbf{M}^4, \tag{3}$$

where a and b are the Landau energy coefficients, T is temperature, and T_c is the Curie temperature. The Landau energy explicitly includes temperature-related magnetization change, which can further influence other energies such as exchange and DMI energies. Then, the exchange energy density can be expressed as

$$\begin{aligned} f_{\text{exch}} = A(&M_{1,1}^2 + M_{1,2}^2 + M_{1,3}^2 + M_{2,1}^2 + M_{2,2}^2 + M_{2,3}^2 \\ &+ M_{3,1}^2 + M_{3,2}^2 + M_{3,3}^2), \end{aligned} \tag{4}$$

where A is the exchange energy coefficient and $M_{i,j} = \partial M_i/\partial x_j$ denotes the derivative of magnetization M_i with respect to x_j. The bulk-type DMI energy density is written as

$$\begin{aligned} f_{\text{DM}} = D(&M_1 M_{3,2} - M_1 M_{2,3} + M_2 M_{1,3} - M_2 M_{3,1} \\ &+ M_3 M_{2,1} - M_3 M_{1,2}), \end{aligned} \tag{5}$$

where D is the DMI constant. The magnetostatic energy density is expressed as

$$\begin{aligned} f_{\text{mag}} = -\frac{\mu_0}{2}(&H_1^2 + H_2^2 + H_3^2) - \mu_0(H_1 M_1 \\ &+ H_2 M_2 + H_3 M_3), \end{aligned} \tag{6}$$

where H_i represent the magnetic field intensity in the material and μ_0 is the vacuum permeability. The elastic energy density including pure elastic energy density and magnetostrictive energy density can be written as

$$\begin{aligned} f_{\text{elas}} = &\frac{1}{2}C_{11}(\varepsilon_{11}^2 + \varepsilon_{22}^2 + \varepsilon_{33}^2) + C_{12}(\varepsilon_{11}\varepsilon_{22} + \varepsilon_{11}\varepsilon_{33} \\ &+ \varepsilon_{33}\varepsilon_{22}) + 2C_{44}(\varepsilon_{12}^2 + \varepsilon_{13}^2 + \varepsilon_{23}^2) \\ &- \frac{3\lambda_{100}}{2M_s^2}(C_{11} - C_{12})(\varepsilon_{11}M_1^2 + \varepsilon_{22}M_2^2 + \varepsilon_{33}M_3^2) \\ &- \frac{6\lambda_{111}}{M_s^2}C_{44}(\varepsilon_{12}M_1M_2 + \varepsilon_{23}M_3M_2 + \varepsilon_{13}M_1M_3), \end{aligned} \tag{7}$$

where C_{11}, C_{12}, and C_{44} are the elastic constants, λ_{100} and λ_{111} are the magnetostrictive coefficients, and M_s is the saturated magnetization.

With the overdamped assumption [44–47], the form of the governing Eq. (1) can be changed as

$$\frac{1}{L}\frac{\partial \mathbf{M}}{\partial t} = -\frac{\delta F}{\delta \mathbf{M}}, \tag{8}$$

where $L = \gamma M_s/\alpha\mu_0$ is the kinetic coefficient of magnetization evolutions. In addition to the LLG equation, the

mechanical equilibrium equation

$$\frac{\partial \sigma_{ij}}{\partial x_j} = \frac{\partial}{\partial x_j}\left(\frac{\partial f}{\partial \varepsilon_{ij}}\right) = 0 \tag{9}$$

and Maxwell's equation

$$\frac{\partial B_i}{\partial x_i} = \frac{\partial}{\partial x_i}\left(-\frac{\partial f}{\partial H_i}\right) = 0 \tag{10}$$

need to be satisfied for the stresses σ_{ij} and magnetic induction B_i in ferromagnetic materials, where x_i and x_j are three coordinates $(i,j = 1-3)$. Although there is no external mechanical load in this work, the strain can be induced by the magnetostrictive effect. Therefore, the elastic energy and mechanical equilibrium equation are included in the calculation model. A nonlinear finite element method is employed to solve the above governing Eqs. (8)–(10). Hu and Wang [48] demonstrated the validity of the Landau energy model for a spin texture like skyrmions. Wang and Wang [40] included the Landau energy in the phase-field model, and calculated static temperature phase diagrams of skyrmions, which are consistent with the experimental phase diagrams [32,33]. Wang *et al*. [22] also reproduced dynamic skyrmion thermal motion observed in experiment [24] by phase-field simulation, which verifies the reliability of the method used in this work.

The material system of this study is a ferromagnetic MnSi thin film of 200, 100, and 5 nm in length, width, and thickness directions, which are set along the x, y, and z directions of Cartesian coordinates, respectively. The origin of the coordinates is located at the center of the thin film, and material parameters of MnSi used for calculations are shown in the Appendix.

III. RESULTS AND DISCUSSION

A. The temperature-related skyrmion-skyrmion interaction

In the ferromagnetic thin film, isolated skyrmions are stable under an appropriate out-of-plane magnetic field. In experiments, a magnetic force microscope tip [49] can further provide a local out-of-plane magnetic field and then induce the emergence of an individual skyrmion and control its position. Following this concept, we apply a local out-of-plane magnetic field to create two isolated skyrmions, and force them close to each other at a short distance like in Fig. 1. The global out-of-plane magnetic field $H_z = -3 \times 10^5$ A/m. The distance between two skyrmions d is defined as the distance between their centers. The skyrmion center and diameter are determined based on the magnetization profile, which follows previous publications [50,51]. When d is small, two skyrmions have large repulsive interaction. After removing the initializing local magnetic fields, the two skyrmions repel each other, and the distance between them increases until they are far enough apart such that the repulsive interaction of them becomes nearly zero.

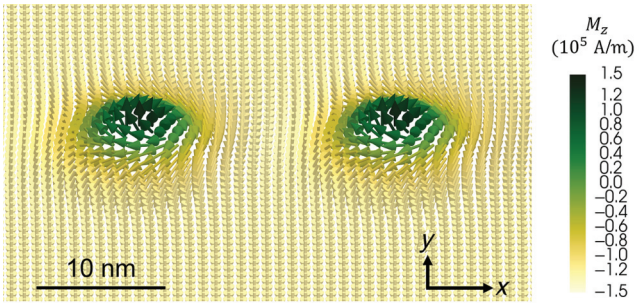

FIG. 1. Schematic of two isolated skyrmions at a short distance apart in MnSi thin film. The distance of the two skyrmions d is defined as the distance between their centers.

From the viewpoint of thermodynamics, the stable state has the lowest free energy as a ground state, while the initial state with two close skyrmions has higher system energy. During the repulsion of skyrmions, the system energy is decreasing until the ground state. Therefore, the extra energy caused by the short distance between skyrmions is defined as the interaction potential U, which can quantitively evaluate the repulsive force of isolated skyrmions [30,31]. In this work, we set two initial skyrmions with a short distance between them and then track the energy change of the system during the relaxation of the two skyrmions, until the system energy does not change as a ground-state energy of the system. Then, by subtracting the ground-state energy from the system energy, the interaction potential U caused by skyrmion-skyrmion interaction is obtained. Based on that, we calculate the interaction potential U for different skyrmion distance d, and compare the results at different system temperatures in Fig. 2. The result shows that two close skyrmions have large repulsive interaction, and the interaction potential becomes zero when the skyrmion distance d becomes large. The marked decrease of U with an increase of d follows an exponential relationship $U(d) \propto \exp(-d/\lambda)$, which is consistent with previous reports [13,14]. Further, the temperature has a great influence on the skyrmion-skyrmion interactions. Generally, at the same skyrmion distance d, the higher the temperature, the smaller the skyrmion interaction. When we focus on the $d = 20$-nm cases, the interaction potential U at 15, 17.5, and 20 K is 10.78×10^{-22}, 4.2×10^{-22}, and 1.35×10^{-22} J, respectively. The interaction potential increases by around 8 times when temperature drops by only 5 K, which indicates that the temperature is a quite significant factor for the skyrmion-skyrmion interaction. Although this result only shows the change of interaction between two skyrmions, it may have implications for a number of effects such as skyrmion ordering [52], melting,

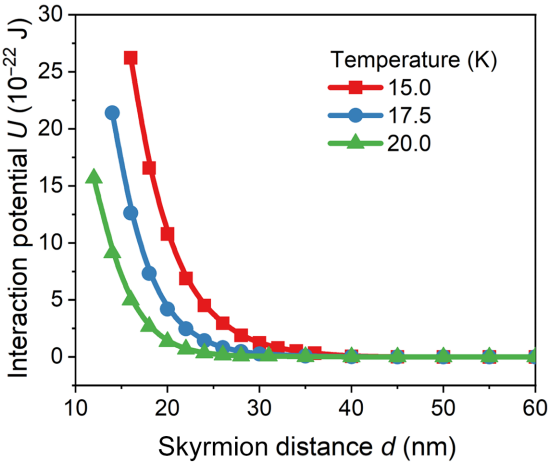

FIG. 2. The interaction potential U for different skyrmion distance d, and comparison at different system temperatures. The prompt decrease of U with an increase of d follows an exponential relationship, $U(d) \propto \exp(-d/\lambda)$, and at the same skyrmion distance d, the higher the temperature, the smaller the skyrmion interaction.

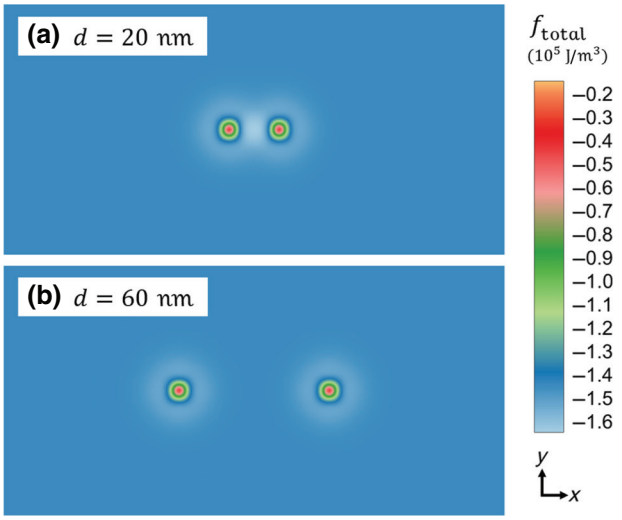

FIG. 3. The system energy density of the thin film with two skyrmions at 15 K. (a) Skyrmion distance $d = 20$ nm. Two skyrmion structures are overlapped and asymmetric, which yields interaction potential U. (b) Skyrmion distance $d = 60$ nm. Two skyrmion structures are isolated and symmetric, for which U is zero.

pinning [53], and motions [54–57] in skyrmion systems in general. For example, a previous study demonstrated that a decreased particle-particle interaction (such as vortex interaction [58] or skyrmion interaction [59]) will increase the pinning effect. Intriguingly, a recent experiment [60] found that the critical depinning current of skyrmions rapidly grows with increasing temperature, which also in turn supports our conclusion, i.e., skyrmion interaction decreases rapidly with an increase of temperature.

B. The mechanism of the temperature-related interaction potential

To reveal the mechanism of the temperature effect on skyrmion-skyrmion interaction, the thermodynamic explanation of skyrmion-skyrmion interaction is discussed first. The system energy density of the thin film with two skyrmions at 15 K is shown in Fig. 3. In Fig. 3(b), the homogeneous blue area is the uniform FM state, in which all magnetizations are parallel to the $-z$ direction of the external field. The core area of the skyrmion state has higher energy density than FM state, which suppresses the nucleation of skyrmions. Therefore, only two preinduced isolated skyrmions exist at the background FM state. Nevertheless, the peripheral area of isolated skyrmions (colored in light blue) has lower energy density than background FM state, which protects the stability of two preinduced skyrmions. Then, when two skyrmions are close at a short distance $d = 20$ nm as in Fig. 3(a), the skyrmion structures are overlapped and deformed. Especially, the peripheral lower-energy area is overlapped, which increases the system energy. This increased part of energy is the interaction potential U. The existence of U is the driving force of the repulsive effect of skyrmions. The repulsive interaction becomes zero when the two skyrmions are totally isolated and symmetric, for which U is zero like in Fig. 3(b).

To further trace the origin of the interaction potential U, we discuss the separate U from the different components of free energies. The components of U are defined as $U = U_{\text{Landau}} + U_{\text{exch}} + U_{\text{DM}} + U_{\text{mag}} + U_{\text{elas}}$, where U_{Landau} to U_{elas} are the interaction potentials from the Landau, exchange, DMI, magnetostatic, and elastic energies, respectively. As shown in Fig. 4, the DMI potential energy U_{DM} rapidly increases when skyrmions are closer, which dominates the increase of skyrmion interaction potential U. The effects of the other free-energy components are opposite to or trivial compared with the DMI energy. Therefore, the origin of the skyrmion-skyrmion interaction is the DMI.

According to Eq. (5), the DMI energy is related to the chiral distribution of magnetizations. In the FM state, there is no chiral distribution of uniform magnetizations, and therefore the DMI energy is zero. However, in the skyrmion state, the chiral magnetization structure yields negative DMI energy for further decreasing the system energy. In Figs. 5(a) and 5(b), the DMI energy density distributions are shown in color map and the skyrmion structures are shown by white arrows. At a short distance ($d = 20$ nm), two skyrmions are overlapped, which makes the chiral magnetization area smaller than two isolated skyrmions. Then, the smaller chiral magnetization area has smaller decreased value of DMI energy, which results an extra system energy (interaction potential). Figures 5(c)

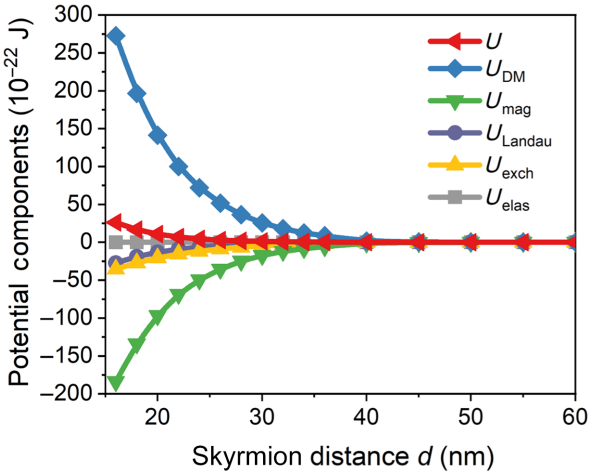

FIG. 4. The separate U from the different components of free energies. The components of U are defined as $U = U_{\text{Landau}} + U_{\text{exch}} + U_{\text{DM}} + U_{\text{mag}} + U_{\text{elas}}$, where U_{Landau} to U_{elas} are the interaction potentials from the Landau, exchange, DMI, magnetostatic, and elastic energies, respectively. The origin of the skyrmion-skyrmion interaction comes from the DMI.

and 5(d) show the detailed magnetization structure of the overlapped and isolated skyrmions, respectively. The overlapped skyrmion indeed loses part of the chiral area then becomes asymmetric, while the isolated skyrmion is intact and symmetric. Therefore, not only the distance and diameter of skyrmions, but also the symmetry of skyrmions is an index to reflect the overlap level of two skyrmions. In conclusion, we find that the interaction potential is from the overlapped skyrmion structure inducing extra DMI energy.

Based on this understanding, the mechanism of the temperature effect of skyrmion-skyrmion interaction can be explained by the skyrmion structures. Figure 6(a) shows the magnetization distributions of two skyrmions at different temperatures (skyrmion distance $d = 20$ nm) and Fig. 6(b) shows the detailed results of Fig. 6(a) for the central axis ($y = 0$). Firstly, the average magnetization magnitude is smaller at higher temperature (17.5 K) than lower temperature (15 K). It directly decreases the value of the system energy and interaction potential, even with the same chiral magnetization structure. Secondly, the skyrmion structure, especially the overlap level of two skyrmions, is also changed by temperature. According to the previous discussion, the overlap level of two skyrmions is related to their distance, diameter, and asymmetry. Here, the distance of skyrmions is the same (20 nm), but the skyrmion diameter is changed by temperature. Our simulation shows that the skyrmion diameters at 15, 17.5, and 20 K are 6.834, 6.208, and 5.459 nm, respectively. Therefore, the overlapped area of two skyrmions is decreased due to the decrease of skyrmion diameter. Further, Fig. 6(b) demonstrates that a skyrmion at higher temperature has

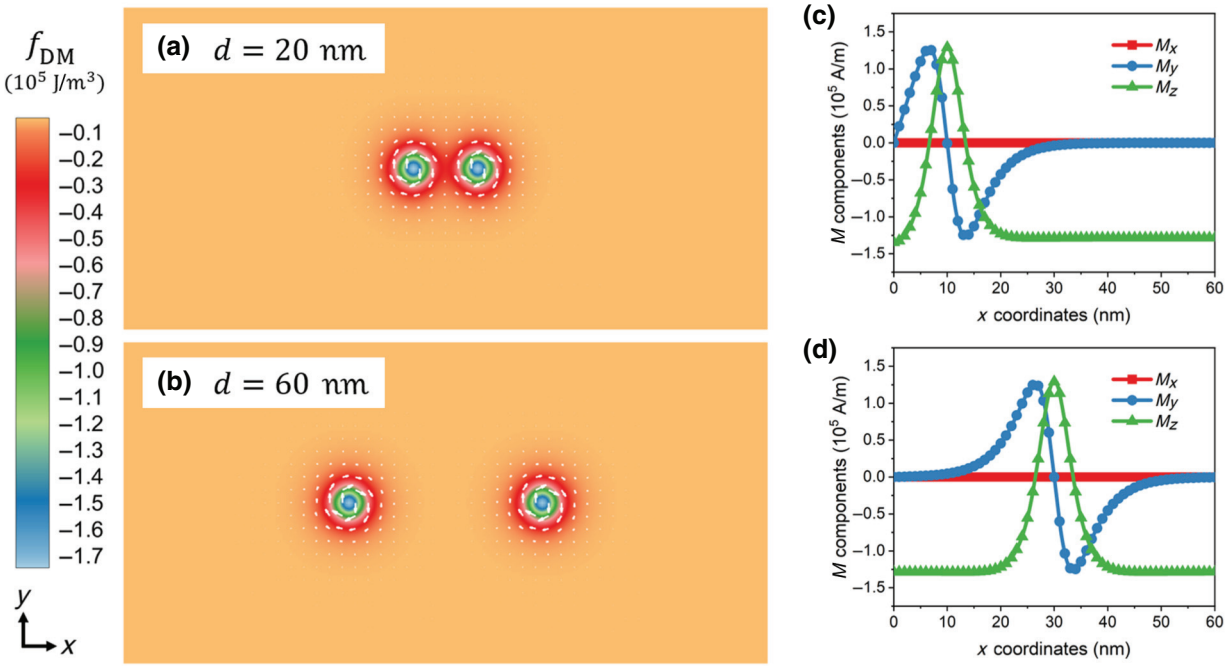

FIG. 5. The distribution of DMI energy density (by color map) and magnetization structures of two skyrmions (by white arrows). (a) The results of short distance $d = 20$ nm and (b) the results of long distance $d = 60$ nm. The magnetization structure of (c) an overlapped skyrmion and (d) an isolated skyrmion. The overlapped skyrmion has a smaller diameter and asymmetric structure, while the isolated skyrmion has a larger diameter and symmetric structure.

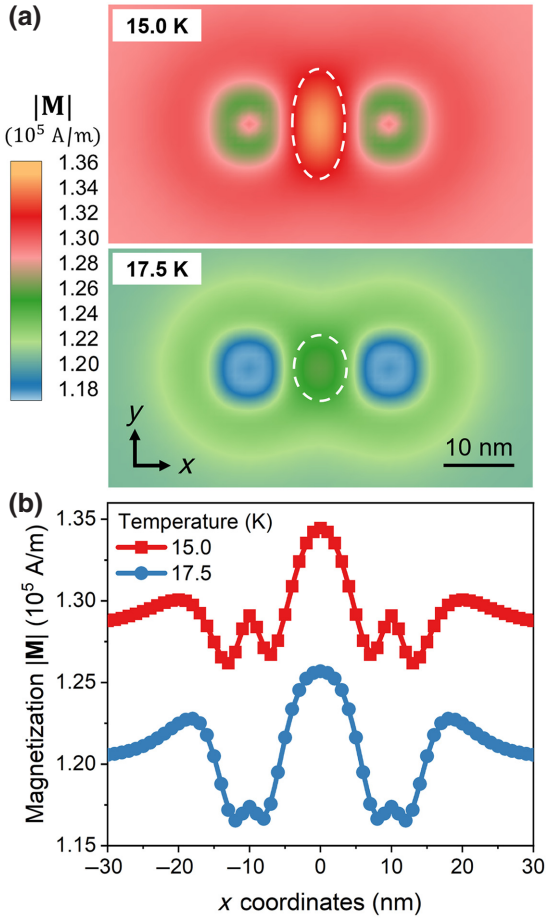

FIG. 6. (a) The magnetization distributions of two skyrmions at different temperatures (with distance $d = 20$ nm). The areas indicated by white dashes show the overlapped areas of two interacting skyrmions. (b) The magnetization along the central axis ($y = 0$) of two skyrmions at different temperatures (15 and 17.5 K).

smaller asymmetry. By comparing the magnetization of both sides of a skyrmion ($x = 0$ and -20), we find the differences of magnetization are 3.26% and 2.55% at 15 and 17.5 K, respectively. Therefore, a less asymmetric skyrmion structure at higher temperature further decreases the overlap area, thus decreasing the interaction potential. In other words, at higher temperature, both magnetization magnitude and overlapped area of skyrmions are decreased [intuitively shown by white dashed areas in Fig. 6(a)], which decreases the interaction potential accordingly. This conclusion is consistent with the result in Fig. 2, and provides the mechanism of temperature-related skyrmion interaction from the viewpoint of thermodynamic skyrmion structures.

It is worth mentioning that the magnetization magnitude inside the overlapped area (where magnetization configuration is noncollinear) is larger than the FM background. Because the DMI energy favors the noncollinear magnetization structure, the magnetization magnitude in this area is increased for further energy minimization. The DMI provides the possibility for an increase of magnetization magnitude inside the chiral area of a skyrmion, but the actual magnetization magnitude is the result of the competition of several free energies such as from DMI and exchange interaction. Such magnetization fluctuations at finite temperatures are already proved in a previous magnetic-domain-wall case [61].

C. The equation of the skyrmion interaction at finite temperatures

Finally, we propose a particle model equation to describe the temperature-related skyrmion-skyrmion interaction. In previous reports [13,14], although the distance-related skyrmion-skyrmion interaction is contributed by skyrmion inner structures, a particle model equation has been proposed to describe the distance-related interaction potential based on the exponential form as $U(d) \propto \exp(-d/\lambda)$. The skyrmion is considered as a particle in the equation, which does not show the specific structure status, and the distance between two skyrmions d is the only independent variable. To show the specific relationship of interaction potential U and temperature T, the $U(T)$ curves are shown in Fig. 7(a). In this figure, the skyrmion distance is 20 nm. At first, with an increase of temperature, the interaction potential decreases sharply due to the decrease of DMI energy. Then, two skyrmions vanish when the temperature reaches 25 K; therefore, the interaction potential becomes zero. In the case where skyrmion distance is relatively large, with increased temperature, the interaction may become zero at a critical temperature reached before the skyrmions vanish. But both cases follow similar $U(T)$ curve because U is very small near both critical temperature and skyrmion vanishing temperature. By comparing Fig. 7(a) with Fig. 4, we find a similar relationship of $U(T)$ and $U(d)$, which indicates that the relationship between skyrmion-skyrmion interaction potential and temperature also follows the exponential form just like interaction potential and distance. Mathematically, the relationship can be expressed as $U(T) \propto \exp(-T/\lambda^*)$, where λ^* is a material parameter. Besides, the temperature T and the skyrmion distance d are demonstrated to be two independent variables from the energy analysis in the previous section. So, we propose a particle model of skyrmion-skyrmion interaction at finite temperatures as

$$U(d, T) = ke^{-[(d/\lambda)+(T/\lambda^*)]}, \tag{11}$$

where k is a material parameter. Then, the skyrmion-skyrmion interactions in the MnSi thin film of this study are an example to demonstrate the accuracy of Eq. (11). Material parameters of Eq. (11) can be obtained by simulation data. For example, λ is fitted by the data of different

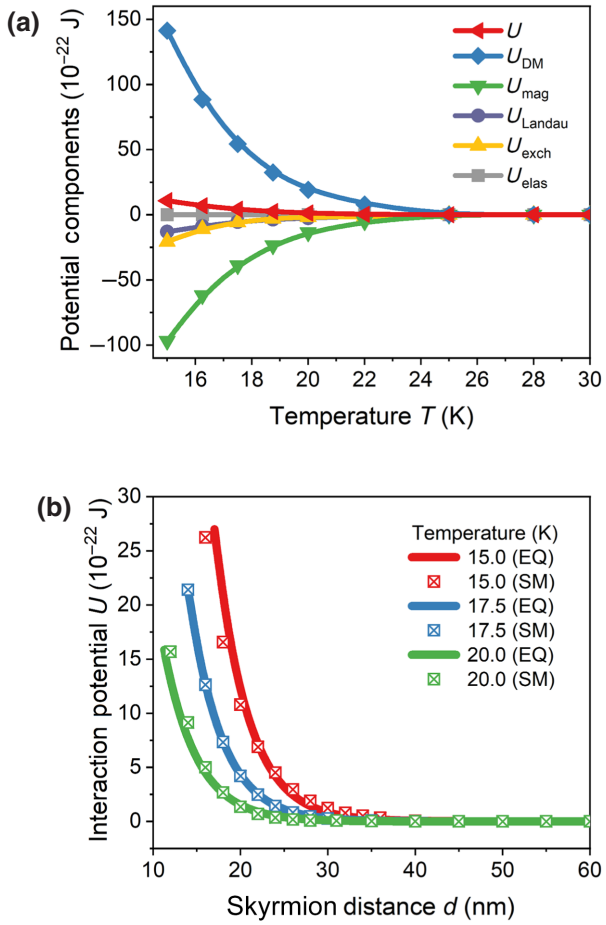

FIG. 7. (a) The $U(T)$ curves, showing the relationship between interaction potential and system temperature. (b) Comparison of $U(d, T)$ between the results of Eq. (11) (EQ) and phase-field simulations (SM), where the lines and square symbols represent the results of the equation and phase-field simulations, respectively.

skyrmion distance d with a fixed temperature, and λ^* is fitted by different temperature T with same distance (the value of fitting parameters are shown in the Appendix). Figure 7(b) shows a comparison of the skyrmion-skyrmion interaction potential $U(d, T)$ between the results of Eq. (11) and phase-field simulations, where the lines and square symbols represent the results of the equation and phase-field simulations, respectively. The results show that Eq. (11) is very well consistent with the simulation at different skyrmion distance d and system temperature T. Therefore, we successfully build a particle model equation that describes the skyrmion-skyrmion interaction at finite temperatures. Although it is derived from two skyrmions, it may be extended to multiple skyrmion systems by summing all of the interaction potentials affecting the ith skyrmion via the relationship $U_i = U_{i,1} + U_{i,2} + \ldots$, where U_i is the total interaction potential of the ith skyrmion and $U_{i,j}$ is the interaction potential between ith and j th skyrmions. This relationship is widely employed in particle models of skyrmion interactions [13] and particle model simulations [58].

IV. CONCLUSION

In summary, we employ a phase-field simulation based on Ginzburg-Landau theory to study the temperature effect on skyrmion-skyrmion interaction. The repulsive interaction of skyrmions decreases sharply with an increase of system temperature. Although we focus on the repulsive interaction here, the attractive interaction should also be influenced by different temperatures. The overlap area of two skyrmions is smaller at higher temperatures, and therefore the annihilation distance of attractive skyrmion-skyrmion interaction should decrease. Based on the simulations, an exponential equation is proposed for describing the repulsive driving force of skyrmion interaction with temperature effect. Therefore, we improve the particle model equation of skyrmion driving force with temperature effect. Recently, the particle model of skyrmion dynamic equation, i.e., Thiele equation [62,63], and the related skyrmion simulations of the particle model [52–57] have been well studied. The particle model can efficiently and accurately describe a variety of skyrmion behaviors such as their ordering [52], melting, pinning [53], and motions [54–57]. Our Eq. (11) can be readily included in the particle model equation and simulations for introducing the temperature-related driving force. Therefore, this work is a great complement for skyrmion theory and simulations, which can predict rich skyrmion behaviors and compare with experimental observations. Furthermore, a recent report [13] indicated that the particle model of skyrmion-skyrmion interaction is not only accurate for skyrmions, but also suitable for any two repulsive, localized magnetic objects (such as skyrmions, chiral domain walls, and boundaries or defects of magnetic systems). Therefore, we anticipate that our equation is a more general form of the temperature-related interaction driving force in magnetic systems, and it highlights an intriguing and rich avenue for future research on magnetic dynamics.

ACKNOWLEDGMENTS

The authors acknowledge financial support from JSPS KAKENHI (20H05653, 20H02027, and 20H05190). J.W. acknowledges financial support from Key Research Project of Zhejiang Laboratory (2021PE0AC02).

APPENDIX

The material parameters of MnSi are presented in Table I. The fitting values of material parameters of Eq. (11) of MnSi are $k = 1.298\,792\,897 \times 10^{-16}$ J, $\lambda = 3.730\,378\,483$ nm, and $\lambda^* = 2.410\,270\,244$ K.

TABLE I. The material parameters of MnSi [39,40,48,64,65].

Landau energy coefficients		Curie temperature	
a_0	6.44×10^{-7} J/A^2 m K	T_c	29.5 K
b	3.53×10^{-16} J m/A^4		
Exchange energy coefficient		DMI constant	
A	1.27×10^{-23} J m/A^2	D	1.14×10^{-14} J/A^2
Vacuum permeability		Saturated magnetization	
μ_0	$4\pi \times 10^{-7}$ H/m	M_s	1.63×10^5 A/m
Elastic constants		Magnetostrictive coefficients	
C_{11}	2.83×10^{11} J/m^3	λ_{100}	3.04×10^{-6}
C_{12}	0.64×10^{11} J/m^3	λ_{111}	2.26×10^{-6}
C_{44}	1.17×10^{11} J/m^3		

[1] U. K. Rößler, A. N. Bogdanov, and C. Pfleiderer, Spontaneous skyrmion ground states in magnetic metals, Nature **442**, 797 (2006).

[2] X. Z. Yu, Y. Onose, N. Kanazawa, J. H. Park, J. H. Han, Y. Matsui, N. Nagaosa, and Y. Tokura, Real-space observation of a two-dimensional skyrmion crystal, Nature **465**, 901 (2010).

[3] I. Dzyaloshinsky, A thermodynamic theory of "weak" ferromagnetism of antiferromagnetics, J. Phys. Chem. Solids **4**, 241 (1958).

[4] T. Moriya, Anisotropic superexchange interaction and weak ferromagnetism, Phys. Rev. **120**, 91 (1960).

[5] N. Nagaosa and Y. Tokura, Topological properties and dynamics of magnetic skyrmions, Nat. Nanotechnol. **8**, 899 (2013).

[6] A. Fert, N. Reyren, and V. Cros, Magnetic skyrmions: Advances in physics and potential applications, Nat. Rev. Mater. **2**, 17031 (2017).

[7] S. Heinze, K. Von Bergmann, M. Menzel, J. Brede, A. Kubetzka, R. Wiesendanger, G. Bihlmayer, and S. Blügel, Spontaneous atomic-scale magnetic skyrmion lattice in two dimensions, Nat. Phys. **7**, 713 (2011).

[8] S. Woo, K. Litzius, B. Krüger, M. Y. Im, L. Caretta, K. Richter, M. Mann, A. Krone, R. M. Reeve, M. Weigand, *et al.*, Observation of room-temperature magnetic skyrmions and their current-driven dynamics in ultrathin metallic ferromagnets, Nat. Mater. **15**, 501 (2016).

[9] J. Chen, J. Hu, and H. Yu, Chiral emission of exchange spin waves by magnetic skyrmions, ACS Nano **15**, 4372 (2021).

[10] H. M. Sommermann, H. W. Wyld, and C. J. Pethick, Skyrmion Interactions at Short Distances, Phys. Rev. Lett. **55**, 476 (1985).

[11] A. Jackson, A. D. Jackson, and V. Pasquier, The skyrmion-skyrmion interaction, Nucl. Phys. Sect. A **432**, 567 (1985).

[12] A. Hosaka, M. Oka, and R. D. Amado, Skyrmions and their interactions using the Atiyah-Manton construction, Nucl. Phys., Sect. A **530**, 507 (1991).

[13] R. Brearton, G. Van Der Laan, and T. Hesjedal, Magnetic skyrmion interactions in the micromagnetic framework, Phys. Rev. B **101**, 134422 (2020).

[14] D. Capic, D. A. Garanin, and E. M. Chudnovsky, Skyrmion–skyrmion interaction in a magnetic film, J. Phys.: Condens. Matte **32**, 415803 (2020).

[15] H. Du, X. Zhao, F. N. Rybakov, A. B. Borisov, S. Wang, J. Tang, C. Jin, C. Wang, W. Wei, N. S. Kiselev, Y. Zhang, R. Che, S. Blügel, and M. Tian, Interaction of Individual Skyrmions in a Nanostructured Cubic Chiral Magnet, Phys. Rev. Lett. **120**, 197203 (2018).

[16] K. L. Tiwari, J. Lavoie, T. Pereg-Barnea, and W. A. Coish, Tunable skyrmion-skyrmion binding on the surface of a topological insulator, Phys. Rev. B **100**, 1 (2019).

[17] H. Odawara, O. Morimatsu, and K. Yazaki, A nonstatic approach to skyrmion-skyrmion interaction, Phys. Lett. B **175**, 115 (1986).

[18] W. Jiang, P. Upadhyaya, W. Zhang, G. Yu, M. B. Jungfleisch, F. Y. Fradin, J. E. Pearson, Y. Tserkovnyak, K. L. Wang, O. Heinonen, *et al.*, Blowing magnetic skyrmion bubbles, Science **349**, 283 (2015).

[19] J. Iwasaki, M. Mochizuki, and N. Nagaosa, Current-induced skyrmion dynamics in constricted geometries, Nat. Nanotechnol. **8**, 742 (2013).

[20] S. Zhang and Z. Li, Roles of Nonequilibrium Conduction Electrons on the Magnetization Dynamics of Ferromagnets, Phys. Rev. Lett. **93**, 1 (2004).

[21] A. Manchon and S. Zhang, Theory of spin torque due to spin-orbit coupling, Phys. Rev. B: Condens. Matter Mater. Phys. **79**, 1 (2009).

[22] Y. Wang, T. Shimada, J. Wang, T. Kitamura, and H. Hirakata, The rectilinear motion of the individual asymmetrical skyrmion driven by temperature gradients, Acta Mater. **221**, 117383 (2021).

[23] L. Kong and J. Zang, Dynamics of an Insulating Skyrmion under a Temperature Gradient, Phys. Rev. Lett. **111**, 1 (2013).

[24] Z. Wang, *et al.*, Thermal generation, manipulation and thermoelectric detection of skyrmions, Nat. Electron. **3**, 672 (2020).

[25] J. J. Liang, J. H. Yu, J. Chen, M. H. Qin, M. Zeng, X. B. Lu, X. S. Gao, and J. M. Liu, Magnetic field gradient driven dynamics of isolated skyrmions and antiskyrmions in frustrated magnets, ArXiv (2017).

[26] R. Yanes, F. Garcia-Sanchez, R. F. Luis, E. Martinez, V. Raposo, L. Torres, and L. Lopez-Diaz, Skyrmion motion induced by voltage-controlled in-plane strain gradients, Appl. Phys. Lett. **115**, 1 (2019).

[27] C. Hu, R. Zhao, L. Ji, W. Chen, S. Bandaru, and X. Zhang, A universal law for predicting the motion behaviors of skyrmions under spatially-varying strain field, J. Magn. Magn. Mater. **513**, 166954 (2020).

[28] T. Yokouchi, S. Sugimoto, B. Rana, S. Seki, N. Ogawa, S. Kasai, and Y. Otani, Creation of magnetic skyrmions by surface acoustic waves, Nat. Nanotechnol. **15**, 361 (2020).

[29] W. Jiang, X. Zhang, G. Yu, W. Zhang, X. Wang, M. Benjamin Jungfleisch, J. E. Pearson, X. Cheng, O. Heinonen, K. L. Wang, *et al.*, Direct observation of the skyrmion Hall effect, Nat. Phys. **13**, 162 (2017).

[30] M. Kutschera and C. J. Pethick, The short-range interaction between skyrmions, Nucl. Phys. A **440**, 670 (1985).

[31] U. B. Kaulfuss and U. Meissner, Deformation effects in the skyrmion-skyrmion interaction, Phys. Rev. D **31**, 3024 (1985).

[32] S. Mühlbauer, B. Binz, F. Jonietz, C. Pfleiderer, A. Rosch, A. Neubauer, R. Georgii, and P. Böni, Skyrmion lattice in a chiral magnet, Science **323**, 915 (2009).

[33] A. Fert, V. Cros, and J. Sampaio, Skyrmions on the track, Nat. Nanotechnol. **8**, 152 (2013).
[34] A. O. Leonov and A. N. Bogdanov, Crossover of skyrmion and helical modulations in noncentrosymmetric ferromagnets, New J. Phys. **20**, 43017 (2018).
[35] H. Wilhelm, M. Baenitz, M. Schmidt, U. K. Rößler, A. A. Leonov, and A. N. Bogdanov, Precursor Phenomena at the Magnetic Ordering of the Cubic Helimagnet FeGe, Phys. Rev. Lett. **107**, 1 (2011).
[36] E. Moskvin, S. Grigoriev, V. Dyadkin, H. Eckerlebe, M. Baenitz, M. Schmidt, and H. Wilhelm, Complex Chiral Modulations in FeGe Close to Magnetic Ordering, Phys. Rev. Lett. **110**, 1 (2013).
[37] C. Pappas, L. J. Bannenberg, E. Lelièvre-Berna, F. Qian, C. D. Dewhurst, R. M. Dalgliesh, D. L. Schlagel, T. A. Lograsso, and P. Falus, Magnetic Fluctuations, Precursor Phenomena, and Phase Transition in MnSi under a Magnetic Field, Phys. Rev. Lett. **119**, 1 (2017).
[38] L. D. Landau and E. M. Lifshitz, *Electrodynamics of Continuous Media* (Pergamon Press, Oxford, 1961).
[39] Y. Wang, J. Sun, T. Shimada, H. Hirakata, T. Kitamura, and J. Wang, Ferroelectric control of magnetic skyrmions in multiferroic heterostructures, Phys. Rev. B **102**, 14440 (2020).
[40] Y. Wang and J. Wang, The temperature-strain phase diagrams of ferromagnetic thin films under different magnetic fields, J. Phys.: Condens. Matter **33**, 235802 (2021).
[41] T. L. Gilbert, A phenomenological theory of damping in ferromagnetic materials, IEEE Trans. Magn. **40**, 3443 (2004).
[42] L. Landau and E. Lifshits, On the theory of the dispersion of magnetic permeability in ferromagnetic bodies, Phys. Z. Sowjetunion **8**, 153 (1935).
[43] M. Lakshmanan and K. Nakamura, Landau-Lifshitz Equation of Ferromagnetism: Exact Treatment of the Gilbert Damping, Phys. Rev. Lett. **53**, 2497 (1984).
[44] J. Wang and J. Zhang, A real-space phase field model for the domain evolution of ferromagnetic materials, Int. J. Solids Struct. **50**, 3597 (2013).
[45] A. Gordon, I. D. Vagner, and P. Wyder, Kinetics of diamagnetic phase transitions, Phys. Rev. B **41**, 658 (1990).
[46] Y. Ni, L. He, and A. G. Khachaturyan, Equivalency principle for magnetoelectroelastic multiferroics with arbitrary microstructure: The phase field approach, J. Appl. Phys. **108**, 023504 (2010).
[47] X. Lu, H. Li, and B. Wang, Theoretical analysis of electric, magnetic and magnetoelectric properties of nano-structured multiferroic composites, J. Mech. Phys. Solids **59**, 1966 (2011).
[48] Y. Hu and B. Wang, Unified theory of magnetoelastic effects in B20 chiral magnets, New J. Phys. **19**, 123002 (2017).
[49] S. Zhang, J. Zhang, Q. Zhang, C. Barton, V. Neu, Y. Zhao, Z. Hou, Y. Wen, C. Gong, O. Kazakova, *et al.*, Direct writing of room temperature and zero field skyrmion lattices by a scanning local magnetic field, Appl. Phys. Lett. **112**, 132405 (2018).
[50] L. Liu, W. Chen, and Y. Zheng, Current-Driven Skyrmion Motion beyond Linear Regime: Interplay between Skyrmion Transport and Deformation, Phys. Rev. Appl. **14**, 1 (2020).
[51] Y. Wang, T. Kitamura, J. Wang, H. Hirakata, and T. Shimada, Mechanical Acceleration and Control of the Thermal Motion of a Magnetic Skyrmion, Phys. Rev. Appl. **18**, 14049 (2022).
[52] J. Stidham and M. Pleimling, Late stages in the ordering of magnetic skyrmion lattices, Phys. Rev. B **102**, 144434 (2020).
[53] L. Xiong, B. Zheng, M. H. Jin, and N. J. Zhou, Collective transport properties of skyrmions on the depinning phase transition, Phys. Rev. B **100**, 1 (2019).
[54] C. Reichhardt, D. Ray, and C. J. Reichhardt, Collective Transport Properties of Driven Skyrmions with Random Disorder, Phys. Rev. Lett. **114**, 1 (2015).
[55] C. Reichhardt and C. J. O. Reichhardt, Thermal creep and the skyrmion Hall angle in driven skyrmion crystals, J. Phys.: Condens. Matter **31**, 07LT01 (2019).
[56] B. L. Brown, U. C. Täuber, and M. Pleimling, Skyrmion relaxation dynamics in the presence of quenched disorder, Phys. Rev. B **100**, 1 (2019).
[57] X. Gong, H. Y. Yuan, and X. R. Wang, Current-driven skyrmion motion in granular films, Phys. Rev. B **101**, 1 (2020).
[58] C. J. Olson, C. Reichhardt, and S. Bhattacharya, Critical depinning force and vortex lattice order in disordered superconductors, Phys. Rev. B: Condens. Matter Mater. Phys. **64**, 245181 (2001).
[59] C. Reichhardt and C. J. Olson Reichhardt, Depinning and nonequilibrium dynamic phases of particle assemblies driven over random and ordered substrates: A review, Rep. Prog. Phys. **80**, 026501 (2017).
[60] T. Schulz, R. Ritz, A. Bauer, M. Halder, M. Wagner, C. Franz, C. Pfleiderer, K. Everschor, M. Garst, and A. Rosch, Emergent electrodynamics of skyrmions in a chiral magnet, Nat. Phys. **8**, 301 (2012).
[61] D. Hinzke, N. Kazantseva, U. Nowak, O. N. Mryasov, P. Asselin, and R. W. Chantrell, Domain wall properties of FePt: From Bloch to linear walls, Phys. Rev. B: Condens. Matter Mater. Phys. **77**, 1 (2008).
[62] S. Z. Lin, C. Reichhardt, C. D. Batista, and A. Saxena, Particle model for skyrmions in metallic chiral magnets: Dynamics, pinning, and creep, Phys. Rev. B: Condens. Matter Mater. Phys. **87**, 1 (2013).
[63] M. Weißenhofer, L. Rózsa, and U. Nowak, Skyrmion Dynamics at Finite Temperatures: Beyond Thiele's Equation, Phys. Rev. Lett. **127**, 47203 (2021).
[64] J. M. Hu, T. Yang, and L. Q. Chen, Stability and dynamics of skyrmions in ultrathin magnetic nanodisks under strain, Acta Mater. **183**, 145 (2020).
[65] J. Miltat, S. Rohart, and A. Thiaville, Brownian motion of magnetic domain walls and skyrmions, and their diffusion constants, Phys. Rev. B **97**, 1 (2018).